Understanding the Metal-Carbon Interface in FePt Catalyzed Carbon Nanotubes

D. Pohl,[1,*] F. Schäffel,[1,†] M. H. Rümmeli,[1] E. Mohn,[1] C. Täschner,[1] L. Schultz,[1] C. Kisielowski,[2] and B. Rellinghaus[1,‡]

[1]*IFW Dresden, P.O. Box 270116, D-01171 Dresden, Germany*

[2]*National Center for Electron Microscopy, Lawrence Berkeley National Laboratory, Berkeley, California 94720, USA*

(Received 11 February 2011; published 25 October 2011)

Any tip functionalization of carbon nanotubes, for which the relative orientation between their (metallic) catalyst particle and the nanotube axis is essential, requires a detailed knowledge of the nature of the internal interface between the particle and the outgrown tube. In the present work, this interface is characterized with atomic precision using state-of-the-art low-voltage aberration-corrected transmission electron microscopy in combination with molecular dynamics simulations for the case of hard-magnetically terminated carbon nanotubes. Our results indicate that the physical principle based upon which the interfacial metal facet is chosen is a reduction of the desorption energy for carbon.

DOI: 10.1103/PhysRevLett.107.185501 PACS numbers: 61.48.De, 61.46.Df, 68.35.−p, 68.37.Og

Since their discovery by Iijima in 1991, carbon nanotubes (CNTs) have stimulated rapidly expanding research because of potential technological application including their use in electronics or as sensors [1–6]. An enhanced lateral resolution in magnetic force microscopy when using ferromagnetically filled CNTs as magnetic tips [7,8], the construction of nanoscale mechanical actuators [9,10], or the realization of nanorelay concepts [11,12] are examples for the technological impact of CNTs. The perspective to functionalize the CNT ends has nourished hopes for constructing novel CNT architectures and networks for nanoelectromechanical systems or simply for substituting functional elements of microscale dimensions by even smaller nanostructures for improved performance. Obviously, control over the CNT growth and their functionalization is of critical importance in such efforts.

In this Letter, the atomic structure of the metal-carbon interface of CNTs with magnetically functionalized tips is revealed. Apparently, magnetic functionalization provides additional design flexibility by exerting a mechanical force (or torque) on CNTs through the application of external magnetic fields. Here, FePt in the chemically ordered intermetallic $L1_0$ phase is particularly promising, since its large magnetic anisotropy and its resistance to oxidation allow for the production of the smallest stable ferromagnets [13]. Recently, we have reported the successful preparation of $L1_0$-FePt-terminated CNTs with mean magnetic switching fields as high as $\mu_0 H_S = 2.5$ T [14]. Only if the orientation of the [001] easy axes of magnetization with respect to the CNT axes can be controlled, magnetic functionalization can be effectively exploited. This demand represents a general and yet unsolved problem in the research on CNT. In order to understand and control the relative orientation of the crystal lattice of the catalyst particle and the CNT axis, a detailed microscopic picture of the CNT growth mechanisms is mandatory. Although this problem has been at the center of CNT research for two decades, such a picture is not yet available. Likewise unknown are the physical principles which rule the choice of a particular facet that forms the metal-carbon interface. As the CNT growth process is intimately related to this interface, a thorough investigation of the nature of the interface seems consequential. Owing to the large variety of CNT synthesis, different and (partially) competing growth models exist [15–20]. In the most widely used preparation process of chemical vapor deposition (CVD), the choice of transition metal catalyst particles provides a degree of control over the CNT morphology, the production yield, and the growth mode itself (base growth vs tip growth) [21,22]. Consequently, the interface between the catalyst particle and the CNT is considered to play a key role for the CNT growth [17,23–26]. Only a few studies deal with the physical properties of these facets which are found to be particularly effective in dissociating the gaseous hydrocarbon feedstock during growth and which typically provide low activation energies for surface diffusion [17,27]. *Ab initio* calculations on interfaces between single-wall CNTs and selected metal surfaces reveal the covalent character of the chemical binding and surprisingly high bond strengths [25]. For single-wall CNT growth the adhesion between the catalyst particle and the graphene cap is stated to be the most important point for the cap lift-off [18–20]. Koziol *et al.* showed a strong relation between an iron-carbide particle and the radial nanotube layer in multiwall CNTs (MWCNTs) grown by the CVD process [28]. Studies of different crystallographic facets of the catalyst and, in particular, for interconnects to MWCNTs are still lacking.

The structure of the internal metal-carbon interface of $L1_0$-FePt-terminated CNTs grown from FePt catalyst particles through plasma-enhanced CVD [14,29] is investigated by means of low-voltage (80 kV), monochromated, aberration-corrected high-resolution transmission electron microscopy (HRTEM) using the ''Team 0.5'' microscope [30].

As an example, Fig. 1(a) shows a HRTEM image of the tip section of a MWCNT terminated with a FePt catalyst particle. The Fourier transform of the particle (FFT, cf. inset) reveals that the particle exhibits the ordered $L1_0$ structure and is oriented with its [110] zone axis parallel to the electron beam (i.e., perpendicular to the image plane). The [001] easy axis of magnetization lies within the image plane as indicated by the white arrow. Figure 1(b) shows a magnification of the metal-carbon interface region. The strong differences between the scattering strengths of the heavy Fe and Pt atoms and the light C atoms provide a criterion based on which the atomic columns may be clearly attributed to either C or Fe/Pt from merely analyzing the image intensity (i.e., the gray value). Figures 2(b) and 2(c) show intensity profiles obtained from the interface region. In these profiles, two different regions with small signal oscillations on a high background and with strong oscillations on a low background can be clearly distinguished. In the FePt particle where the atoms are stacked in columns, pronounced channeling of the electron wave occurs which leads to intense peaks on a low background [31,32]. In contrast, in the CNT, the atoms are not stacked within columns and as a consequence, electron channeling is largely reduced, which leads to a very diffuse image contrast (i.e., weak oscillations on a high background). Based on this criterion, the interface between the metallic catalyst and the CNT can be determined from such profiles with atomic precision. This analysis allows us to identify those atoms of the FePt particle which form the metal-carbon interface. Accordingly in Fig. 1(b), interface atom columns which belong to {111} facets are labeled light blue, others are labeled yellow. From the HRTEM micrograph and its FFT [Fig. 1(a)] it becomes evident that the four bottommost graphene sheets emanate from a $(\bar{1}11)$ FePt facet.

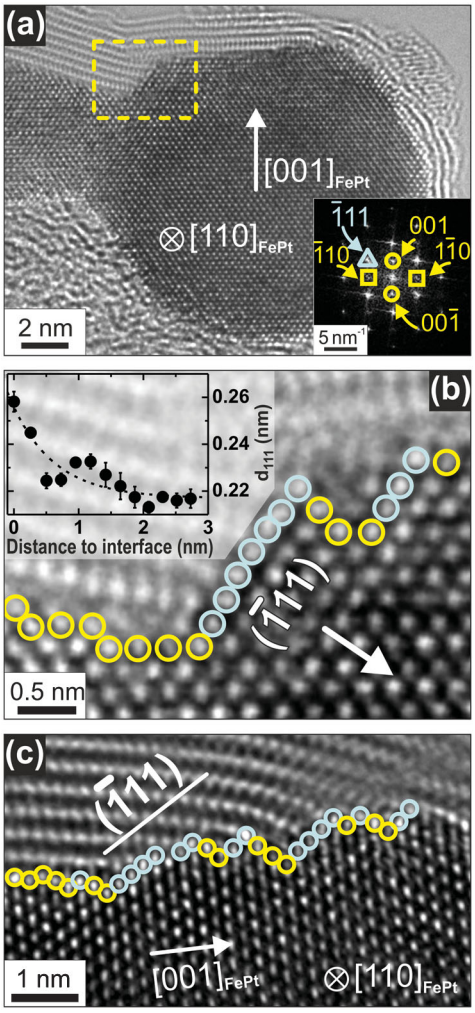

FIG. 1 (color). HRTEM close-up of the internal metal-carbon interface in a FePt-terminated CNT. (a) CNT with its catalyst particle oriented in [110] zone axis. Inset: FFT of the particle region. Symbols correspond to crystallographic directions. Triangle, {111}; circle, {001}; square, {110}. (b) Magnification of the marked region in (a). Atoms which belong to {111} facets are labeled light blue, others yellow. Inset: {111} lattice spacing, d_{111}, as a function of the distance from the interface. The symbols and dashed line represent the experimental data and a fitted decay function, respectively. (c) Tip region of a second FePt-terminated CNT.

Such detailed analysis of the interfacial area is only possible if the catalyst particle lies sufficiently close to a zone axis orientation and is thus limited to only few particles. Nonetheless, investigations on 27 interfaces reveal that carbon *preferentially* ($> 75\%$) emanates from {111} facets. Figure 3 shows that this portion (red data) is by far larger than the experimentally determined occurrence of {111} facets in the FePt catalyst particles themselves (black). It also outnumbers the probability with which {111} facets occur in fcc crystals (left hatched) or terminate truncated octahedra (whose morphology is similar to that of the experimental particles, right hatched), respectively. A pronounced bending of the graphene layers toward the {111} facets is also often found which confirms the origin of the CNT on these particular facets. This finding is important not only since the metal-carbon

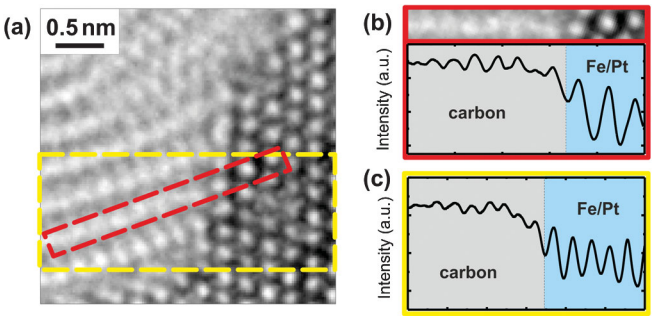

FIG. 2 (color). Determination of the atomic arrangement at the metal-carbon interface. (a) Close-up of the interface region of a CNT. (b) Intensity profile along the projection of an individual graphitic layer of a CNT across the interface. (c) Intensity profile of the entire interface region marked in (a).

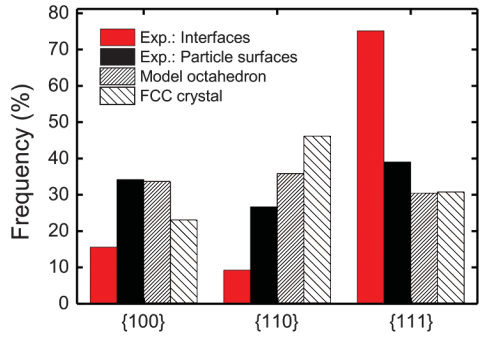

FIG. 3 (color). Analysis of the occurrence of {100}, {110}, and {111} planes at the metal-carbon interfaces (red, 27 interfaces analyzed) and at the visible surfaces of the FePt catalyst particles (black, 19 particles analyzed). The experimental data are compared to the frequency of the occurrence of these planes at the (visible) surfaces of model octahedra (right hatched) and in fcc crystals (left hatched), respectively.

interface determines the relative orientation of the CNT and the crystallographic orientation of the catalyst particle. The carbon-metal interface also affects the chirality of the outgrowing CNT [33–35].

The HRTEM images depicted in Fig. 1 reveal a variety of additional details, such as the occurrence of step edges on the interface, the rooting of the graphene layers on hollow sites of the facets, or a Bernal type AB stacking of the graphene layers within the CNT. These findings only occur in individual cases and *no* preferential growth from step edges nor for a particular rooting or stacking of the CNT are found from the statistical investigation of different CNT. There is also no preferred angle between the {111} facets and the outgrown CNT. Rather the bending seems to be determined by the overall particle morphology and the *radial* metal-carbon interface where carbon diffusion occurs during the CNT growth [28].

In the inset of Fig. 1(b), another characteristic feature of these internal metal-carbon interfaces is presented. Here, the interplanar {111} lattice spacing, d_{111}, is plotted as a function of the distance from the interface. There is a significant increase of the lattice spacing upon approaching the interface which may even exceed 10%. Whereas strain in CNTs as manifested by a bending of the graphene layers is often observed near the interface to the catalyst (see, e.g., [25,26,36]), strain within the catalyst particles themselves is so far scarcely reported, and the details of the atomic structure have not yet been revealed [36]. In FePt nanoparticles, a dilation of the surface-near lattice is known to originate from a segregation of Pt to the particles surface [37]. This Pt segregation is also believed to cause the frequently observed low degree of $L1_0$ order in such particles [37–41].

In order to exclude that in the present case where the metal is in intimate contact with carbon, the observed lattice dilation is due to an interface-near dissolution of carbon, MD simulations on the incorporation of carbon in FePt were conducted. Our simulations have shown that d_{111} grows almost linearly upon increasing the C concentration [29]. To account for the experimentally observed 10% increase of d_{111}, a carbon content of at least 20 at. % is necessary. This largely exceeds the high temperature carbon solubility in γ-Fe [42] and would result in a c/a ratio as low as 0.8 which could be easily measured from the HRTEM images. Here, the c/a ratio was never found to be smaller than c/a (expt.) $\simeq 0.96$. Consequently, the dissolution of C in FePt cannot account for the observed lattice dilation at the metal-carbon interface. Rather it is attributed to the aforementioned Pt segregation.

Additional simulations are conducted to investigate why carbon preferentially emerges from the Pt-rich {111} facets of the FePt catalyst particle. It is first assumed that the observed structures still reflect the (late) CNT growth state. Surface-directed diffusion of carbon along [111] onto the {111} facets is ruled out, since these are the most densely packed atomic planes in cubic and tetragonal crystals. Instead, MD simulations were conducted to estimate the desorption energy (i.e., the adsorption energy) of carbon atoms for various surfaces. For this, single carbon atoms were randomly positioned onto different surfaces and the adsorption energy was estimated from the maximum energy difference between the substrate crystal with and without carbon. For the {111}, {110}, and {100} surfaces of fcc Fe, the obtained adsorption energies are $\epsilon_{111}^{\mathrm{Fe}} = -6.7$ eV, $\epsilon_{110}^{\mathrm{Fe}} = -7.2$ eV, and $\epsilon_{100}^{\mathrm{Fe}} = -7.9$ eV, respectively, whereas for Pt, $\epsilon_{111}^{\mathrm{Pt}} = -3.8$ eV, $\epsilon_{110}^{\mathrm{Pt}} = -5.1$ eV, and $\epsilon_{100}^{\mathrm{Pt}} = -5.0$ eV are clearly smaller. This reflects the stronger chemical binding between Fe and C and is in accordance with the fact that the chemical affinity of an element to carbon is higher the larger its number of unfilled *d* orbitals is. The calculated adsorption energies of around 7 eV/atom for fcc Fe are comparably high as those derived for Ni [23] and fcc Co [25], and as in Ni, the binding is weakest on {111} facets. For the FePt alloy, the values lie between those for elemental Fe and Pt and vary with the number of Fe and/or Pt bonds. Altogether, the MD simulations show that the *lowest* adsorption energy for carbon is provided by the {111} facets of Pt which in turn means that carbon is more easily *released* from {111} Pt. This finding is in very good agreement with the HRTEM investigations which indicate that the concentric graphene layers of the CNT preferentially emanate from Pt-rich {111} facets of the catalyst particle.

Since the characterization was done *ex situ*, one cannot exclude the possibility that the metal-carbon interface was modified upon cooling to room temperature. This would, e.g., be the case when the CNT grow through a vapor-liquid-solid process which involves the (partial) melting of the catalyst [43]. Then the interface observed in the microscope would *not* reflect the CNT growth state and the above drawn conclusion would be invalid. The differences in the adsorption energies among different facets (1.2 eV/at. for

Pt surfaces) are larger than the differences in surface energies (0.3 to 0.6 eV/at. [29]) and thus dominate the energetics of the metal-carbon interface. Consequently, since a change of the interface upon cooling only occurs together with a reduction in energy, thermal equilibration of the interface would be primarily achieved through maximization of the *gain* in adsorption energy which would favors {100} or {110} facets. This scenario is in clear contrast to the observed preference of {111} facets. Alternatively, in order to equilibrate the morphology of (free) FePt nanoparticles, the minimization of the surface energy leads to an energetic preference of {111} and {100} surfaces and thus to the formation of different types of truncated octahedra [44,45]. Indeed is the occurrence of {100}, {110}, and {111} facets on the FePt catalyst particles themselves in good agreement with octahedral particle morphologies (cf. Fig. 3). At the metal-carbon interface, the frequency of the {111} facets is again noticeably high. Consequently, the experimentally determined preference of {111} facets at the metal-carbon interface (i) strongly suggests that the CNT growth state is largely preserved upon cooling to room temperature and (ii) proves the *kinetic* stabilization of the internal metal-carbon interface through minimization of the desorption energy.

In summary, the combination of structural characterization by means of monochromated aberration-corrected low-voltage HRTEM with MD simulations was shown to resolve interfacial structures within CNT with atomic precision and provide valuable insight into the construction principles behind such structures. In FePt-terminated CNT, the concentric graphene layers of the outgrowing CNT are found to preferentially emanate from Pt-enriched {111} facets of the catalyst particles. The physical principle behind this preference is of a kinetic nature, as the chosen facets provide the lowest desorption energy to be paid for the release of carbon atoms from the metal particle during CNT growth. This finding may nourish future efforts to tailor the relative orientation of the CNT axis and the catalyst particle. Epitaxial relations between the catalyst and a (single crystal) substrate could, e.g., be utilized to not only optimize the growth process by providing the kinetically favored interface. A likewise predefined orientation of magnetic catalyst particles with uniaxial anisotropy should then also allow one to control the orientation of the easy axes of magnetization. Such an approach would offer new routes to prepare nanostructured magnetic materials with homogeneous and predefined anisotropy, e.g., for data storage applications.

The authors thank R. Erni for his support at NCEM, Berkeley, R. Kalthofen for coating the CVD substrates, and K. Albe and T. Järvi for their help with the MD simulations. F. S. acknowledges financial support by the Cusanuswerk. Part of the work was performed at NCEM, which is supported by the U.S. Department of Energy (Contract No. DE-AC0205CH11231).

*d.pohl@ifw-dresden.de
†Present address: University of Oxford, Department of Materials, Parks Road, Oxford, OX1 3PH, United Kingdom.
‡b.rellinghaus@ifw-dresden.de

[1] S. Iijima, Nature (London) **354**, 56 (1991).
[2] J. Kong, N. R. Franklin, C. W. Zhou, M. G. Chapline, S. Peng, K. J. Cho, and H. J. Dai, Science **287**, 622 (2000).
[3] J. Li, Y. J. Lu, Q. Ye, M. Cinke, J. Han, and M. Meyyappan, Nano Lett. **3**, 929 (2003).
[4] A. Modi, N. Koratkar, E. Lass, B. Q. Wei, and P. M. Ajayan, Nature (London) **424**, 171 (2003).
[5] S. J. Tans, A. R. M. Verschueren, and C. Dekker, Nature (London) **393**, 49 (1998).
[6] K. Jensen, J. Weldon, H. Garcia, and A. Zettl, Nano Lett. **7**, 3508 (2007).
[7] N. R. Wilson and J. V. Macpherson, Nature Nanotech. **4**, 483 (2009).
[8] S. S. Wong, E. Joselevich, A. T. Woolley, C. L. Cheung, and C. M. Lieber, Nature (London) **394**, 52 (1998).
[9] B. C. Regan, S. Aloni, K. Jensen, R. O. Ritchie, and A. Zettl, Nano Lett. **5**, 1730 (2005).
[10] A. M. Fennimore, T. D. Yuzvinsky, W. Q. Han, M. S. Fuhrer, J. Cumings, and A. Zettl, Nature (London) **424**, 408 (2003).
[11] J. M. Kinaret, T. Nord, and S. Viefers, Appl. Phys. Lett. **82**, 1287 (2003).
[12] D. C. Lee, F. V. Mikulec, and B. A. Korgel, J. Am. Chem. Soc. **126**, 4951 (2004).
[13] D. Weller, A. Moser, L. Folks, M. E. Best, W. Lee, M. F. Toney, M. Schwickert, J. U. Thiele, and M. F. Doerner, IEEE Trans. Magn. **36**, 10 (2000).
[14] F. Schäffel, C. Täschner, M. H. Rümmeli, V. Neu, U. Wolff, U. Queitsch, D. Pohl, R. Kaltofen, A. Leonhardt, B. Rellinghaus, B. Büchner, and L. Schultz, Appl. Phys. Lett. **94**, 193107 (2009).
[15] R. T. K. Baker, Carbon **27**, 315 (1989).
[16] M. H. Rümmeli, F. Schäffel, C. Kramberger, T. Gemming, A. Bachmatiuk, R. J. Kalenczuk, B. Rellinghaus, B. Büchner, and T. Pichler, J. Am. Chem. Soc. **129**, 15 772 (2007).
[17] S. Hofmann, G. Csanyi, A. C. Ferrari, M. C. Payne, and J. Robertson, Phys. Rev. Lett. **95**, 036101 (2005).
[18] H. Kanzow and A. Ding, Phys. Rev. B **60**, 11 180 (1999).
[19] H. Kanzow, C. Lenski, and A. Ding, Phys. Rev. B **63**, 125402 (2001).
[20] M. A. Ribas, F. Ding, P. B. Balbuena, and B. I. Yakobson, J. Chem. Phys. **131**, 224501 (2009).
[21] W. Kim, H. C. Choi, M. Shim, Y. M. Li, D. W. Wang, and H. J. Dai, Nano Lett. **2**, 703 (2002).
[22] T. Yamada, T. Namai, K. Hata, D. N. Futaba, K. Mizuno, J. Fan, M. Yudasaka, M. Yumura, and S. Iijima, Nature Nanotech. **1**, 131 (2006).
[23] W. Xiao, M. I. Baskes, and K. Cho, Surf. Sci. **603**, 1985 (2009).
[24] F. Ding, P. Larsson, J. A. Larsson, R. Ahuja, H. M. Duan, A. Rosen, and K. Bolton, Nano Lett. **8**, 463 (2008).
[25] J. A. Rodriguez-Manzo, F. Banhart, M. Terrones, H. Terrones, N. Grobert, P. M. Ajayan, B. G. Sumpter, V.

Meunier, M. Wang, Y. Bando, and D. Golberg, Proc. Natl. Acad. Sci. U.S.A. **106**, 4591 (2009).
[26] F. Banhart, Nanoscale **1**, 201 (2009).
[27] S. Helveg, C. Lopez-Cartes, J. Sehested, P. L. Hansen, B. S. Clausen, J. R. Rostrup-Nielsen, F. Abild-Pedersen, and J. K. Norskov, Nature (London) **427**, 426 (2004).
[28] K. K. K. Koziol, C. Ducati, and A. H. Windle, Chem. Mater. **22**, 4904 (2010).
[29] See Supplemental Material at http://link.aps.org/supplemental/10.1103/PhysRevLett.107.185501 for details on image and interface analysis, the experimental setup, and simulation conditions.
[30] C. Kisielowski *et al.*, Microsc. Microanal. **14**, 469 (2008).
[31] P. Geuens and D. Van Dyck, Ultramicroscopy **93**, 179 (2002).
[32] S. Van Aert, P. Geuens, D. Van Dyck, C. Kisielowski, and J. R. Jinschek, Ultramicroscopy **107**, 551 (2007).
[33] H. W. Zhu, K. Suenaga, J. Wei, K. Wang, and D. Wu, J. Cryst. Growth **310**, 5473 (2008).
[34] G. Lolli, L. A. Zhang, L. Balzano, N. Sakulchaicharoen, Y. Q. Tan, and D. E. Resasco, J. Phys. Chem. B **110**, 2108 (2006).
[35] Y. Shibuta, Diam. Relat. Mater. **20**, 334 (2011).
[36] J. A. Rodriguez-Manzo, M. Terrones, H. Terrones, H. W. Kroto, L. T. Sun, and F. Banhart, Nature Nanotech. **2**, 307 (2007).
[37] R. M. Wang, O. Dmitrieva, M. Farle, G. Dumpich, H. Q. Ye, H. Poppa, R. Kilaas, and C. Kisielowski, Phys. Rev. Lett. **100**, 017205 (2008).
[38] C. Antoniak, M. Spasova, A. Trunova, K. Fauth, F. Wilhelm, A. Rogalev, J. Minar, H. Ebert, M. Farle, and H. Wende, J. Phys. Condens. Matter **21**, 336002 (2009).
[39] M. Müller and K. Albe, Phys. Rev. B **72**, 094203 (2005).
[40] B. Rellinghaus, S. Stappert, M. Acet, and E. F. Wassermann, J. Magn. Magn. Mater. **266**, 142 (2003).
[41] B. Yang, M. Asta, O. N. Mryasov, T. J. Klemmer, and R. W. Chantrell, Scr. Mater. **53**, 417 (2005).
[42] T. B. Massalski, H. Okamoto, J. L. Murray, L. H. Bennet, and H. Baker, *Binary Alloy Phase Diagrams* (ASM International, Ohio, 1992), 2nd ed.
[43] E. F. Kukovitsky, S. G. L'vov, and N. A. Sainov, Chem. Phys. Lett. **317**, 65 (2000).
[44] B. Rellinghaus, E. Mohn, L. Schultz, T. Gemming, M. Acet, A. Kowalik, and B. F. Kock, IEEE Trans. Magn. **42**, 3048 (2006).
[45] F. Baletto and R. Ferrando, Rev. Mod. Phys. **77**, 371 (2005).